

# Audio-Plane: Audio Factorization Plane Gaussian Splatting for Real-Time Talking Head Synthesis

Shuai Shen<sup>1</sup> Wanhua Li<sup>2</sup> Yunpeng Zhang<sup>3</sup> Weipeng Hu<sup>1</sup> Yap-Peng Tan<sup>1</sup>

<sup>1</sup>Nanyang Technological University <sup>2</sup>Harvard University <sup>3</sup>PhiGent Robotics

## Abstract

Talking head synthesis has become a key research area in computer graphics and multimedia, yet most existing methods often struggle to balance generation quality with computational efficiency. In this paper, we present a novel approach that leverages an Audio Factorization Plane (Audio-Plane) based Gaussian Splatting for high-quality and real-time talking head generation. For modeling a dynamic talking head, 4D volume representation is needed. However, directly storing a dense 4D grid is impractical due to the high cost and lack of scalability for longer durations. We overcome this challenge with the proposed Audio-Plane, where the 4D volume representation is decomposed into audio-independent space planes and audio-dependent planes. This provides a compact and interpretable feature representation for talking head, facilitating more precise audio-aware spatial encoding and enhanced audio-driven lip dynamic modeling. To further improve speech dynamics, we develop a dynamic splatting method that helps the network more effectively focus on modeling the dynamics of the mouth region. Extensive experiments demonstrate that by integrating these innovations with the powerful Gaussian Splatting, our method is capable of synthesizing highly realistic talking videos in real time while ensuring precise audio-lip synchronization. Synthesized results are available in <https://sstzal.github.io/Audio-Plane/>.

## 1. Introduction

Talking head synthesis aims at generating animated facial talking videos that mimic human speech. It has emerged as a pivotal area of research within the fields of computer graphics and multimedia [6, 36, 44, 46, 47].

Recently, the field of talking head synthesis has witnessed substantial research endeavors. These existing works can be broadly categorized into 2D-based methods and 3D-based ones. Predominantly, 2D-based approaches utilize Generative Adversarial Networks (GANs) [8, 11, 14, 21, 23, 27] for audio to lip mapping. However, the lack of

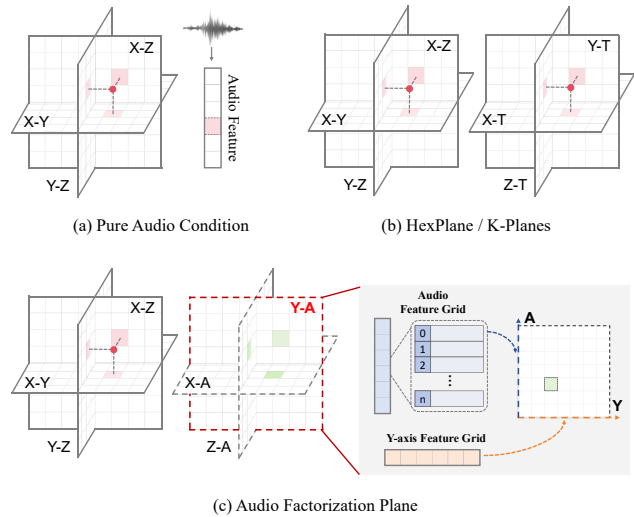


Figure 1. Illustration of the proposed Audio Factorization Plane and two other kinds of representation for dynamic scene modeling.

3D structural modeling limits their ability to generate high-resolution and high-quality talking videos. By contrast, 3D-based methods [15, 18, 19, 32, 33, 42, 48] are known for producing higher-quality talking videos due to their modeling of 3D facial structures. Among them, the commonly used technical frameworks include 3D Morphable Models (3DMM) [1] and Neural Radiance Fields (NeRFs) [25]. However, these methods are often constrained by high computational demands and slow rendering speeds.

Balancing generation quality with computational costs has consistently been a critical theme in the research field of talking head synthesis. More recently, the emergence of Gaussian Splatting [17, 38] provides a new way for real-time 3D-aware rendering. In this paper, we turn attention to this powerful generative technology, and propose an Audio Factorization Plane-based Gaussian Splatting for audio-driven talking face synthesis. For modeling a dynamic talking head, 4D volume representation is needed. However, storing a dense 4D grid is highly resource-intensive and lacks scalability over extended durations. This limitation highlights the need for a more compact and interpretable 4D

volume representation with less redundancy and better scalability. Figure 1 illustrates some 4D scene representations: (a) is the common practice [4, 19, 32], where audio and spatial features are learned separately. This approach explicitly models the 3D spatial field, and relies on an MLP to implicitly learn the audio-conditioned dynamic 4D field, leading to longer optimization time. (b) shows the six-planes [2, 13] to represent the dynamic scene. When applied to talking head modeling, it may perform well for interpolation generation within known temporal contexts, but encounters challenges in extrapolation, thereby limiting its ability to effectively generalize to novel driven audio inputs.

Building on recent advancements in dynamic scene representation [2, 13], we introduce the Audio Factorization Plane (Audio-Plane) as Figure 1 (c). The Audio-Plane is constructed by decomposing the audio-aware 4D volume representation into audio-independent space planes and audio-dependent planes. A key challenge in building the audio-dependent planes is that audio features, unlike spatial coordinates, are not scalar values, making them difficult to represent directly as a dimension. To address this, we further factorize audio-dependent planes into an audio prototype grid and three spatial feature grids. In this way, the audio feature grid pairing with each spatial feature grid can span a feature plane, *e.g.* plane *Y-A* in (c). Notably, *Y-A* is represented with dashed lines, as it is not a true feature plane, but is spanned by two feature grids. This design provides a compact and interpretable audio-driven dynamic scene representation, which enables nuanced audio-spatial interactions. Furthermore, to enhance the dynamic modeling of mouth regions, we introduce the dynamic splatting method to explicitly supervise the dynamism of 3D Gaussian points. Specifically, we assign each Gaussian point with a dynamism weight to construct the deformation field. These weights are then splatted into image space for explicit region-aware deformation supervision, enabling precise control over facial dynamics. By integrating the Audio-Plane and the region-aware dynamic splatting with the Gaussian Splatting backbone, our method can achieve high-fidelity and real-time talking video generation.

Comprehensive experiments show the superiority of the proposed method in rendering quality and speed, which provides a strong baseline for talking head synthesis. To summarize, we make the following contributions:

- We propose the Audio Factorization Plane representation for real-time talking head synthesis, which incorporates temporal audio features with spatial grids and provides a compact audio-driven dynamic scene representation.
- We further develop a dynamic splatting method to explicitly supervise the dynamism of 3D Gaussian points. With explicit region-aware deformation supervision, finer facial motion modeling is achieved.
- The proposed method can generate vivid talking videos in

real time, establishing a strong baseline for high-quality and efficient rendering in talking head synthesis.

## 2. Related Work

**Audio-driven Talking Head Synthesis.** The task of talking head synthesis aims to generate realistic talking videos synchronized with the input audio. Existing approaches can be categorized into 2D-based and 3D-based ones, considering how they model the problem. The 2D-based methods [5, 8, 11, 12, 14, 27, 35, 39] usually treat the problem as a process of audio-to-lip translation. Wav2lip [27] proposed an encoder-decoder CNN model with a well-trained lip-sync expert to generate lip-syncing talking faces. MakeItTalk [47] disentangled the facial information and audio content to enable speaker-aware talking-head animations. However, 2D-based methods, without modeling explicit 3D geometry, can suffer from unstable training and limited facial fidelity. By contrast, 3D-based methods do well in improving the fidelity and consistency of facial animations. A series of studies [30, 31, 34] utilized 3D Morphable Models [1] as the intermediate representations. Recently, Neural Radiance Fields (NeRFs) [25] have been employed as a new popular 3D-aware implicit representation [3, 15, 19, 28, 29, 32, 42]. AD-NeRF [15] proposed the first audio-driven neural radiance field framework for talking-head synthesis. RAD-NeRF [32] developed a decomposed audio-spatial encoding module for talking face modeling. ER-NeRF [19] introduced a tri-plane hash representation coupled with a region attention module for more efficient rendering. Though both methods [19, 32] consider the spatial-aware audio feature, they typically apply audio at a broader level. In comparison, our method factorizes audio into a phoneme prototype feature grid and embeds it with spatial dimensions, allowing for refined audio-spatial interactions. More recently, Gaussian Splatting has emerged as a more computationally efficient generation framework.

**Gaussian Splatting.** Splatting has been an important technique in computer graphics. One of its early applications was in the field of point-based graphics, where SurfaceSplatting [49] demonstrated its utility for surface rendering from point samples, emphasizing its capability to produce high-quality images without the need for complex meshing processes. Within recent advancements in NeRF [25], the Gaussian splatting (GS) techniques were explored for differentiable volumetric rendering [26] to enhance the volumetric representation of 3D scenes. A notable advancement in the field was 3DGS [17], which demonstrated how GS can be effectively utilized to render high-quality radiance fields in real-time. Other works [22, 24, 40, 41, 41] further pushed the boundaries of 3DGS to dynamic scene reconstruction. Representative method 4DGS [38] proposed a HexPlane-based [2] Gaussian deformation field for spatial-temporal modeling. GS has also

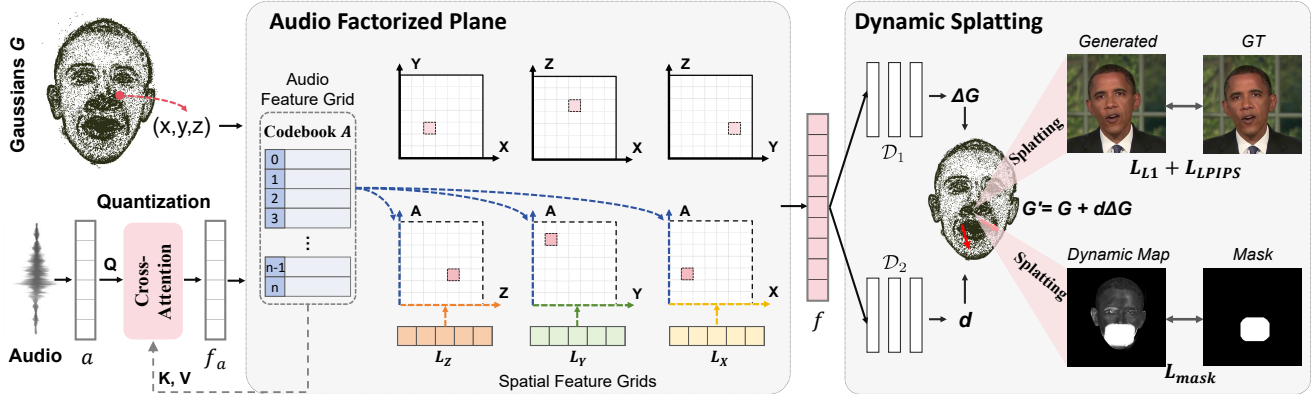


Figure 2. Overview of the proposed Audio-Plane for real-time talking head video synthesis. We develop the Audio Factorized Plane to incorporate audio signals into the feature planes, to strengthen the model for temporally coherent facial motion modeling. We further develop a dynamic splatting method to explicitly supervise the dynamism of 3D Gaussian points, which helps to enhance the modeling of dynamic facial regions while reducing unnecessary complexity in less dynamic areas.

been explored for talking head synthesis task [7, 20, 43]. Cho *et al.* [7] proposed a spatial-audio attention module to facilitate the dynamic deformation of facial regions. Li *et al.* [20] modeled the face and inside mouth branches separately for more efficient training. In contrast, this work focuses on constructing a more compact and interpretable feature representation for audio-driven Gaussian Splatting.

### 3. Methodology

#### 3.1. Overview

In this work, we propose to model the talking head as dynamic audio-driven Gaussians with an Audio Factorization Plane (Audio-Plane), and employ the differentiable splitting operation for high-quality and real-time talking video rendering. An overview of the proposed Audio-Plane is shown in Figure 2. We present the Audio Factorization Plane by decomposing the audio-aware 4D volume representation into audio-independent space planes and audio-dependent planes. The Audio-Plane offers a more compact and interpretable representation of talking faces, strengthening the model’s ability to model temporally consistent facial motion. To further enhance the modeling of mouth regions for improved audio-lip synchronization, we introduce a dynamic splatting technique that enables explicit region-aware dynamism supervision of the unordered Gaussian points. In the following sections, we introduce the proposed dynamic audio-driven Gaussian splatting for talking head synthesis in Section 3.2. In Section 3.3, we explain the proposed Audio Factorization Plane. Section 3.4 details the deformation field. The training objectives are described in Section 3.5.

#### 3.2. Dynamic Gaussian Splatting for Talking Head

This section introduces the proposed Dynamic Gaussian Splatting for Talking Head synthesis. Prior to that, that’s

take a glance at the preliminary 3D Gaussian Splatting framework (3DGS) [17].

**3D Gaussian Splatting.** 3D Gaussian Splatting explicitly represents the scene as a set of 3D point clouds modeled as Gaussian distribution. A 3D Gaussian for a 3D coordinate  $x \in \mathbb{R}^3$  can be defined by a covariance matrix  $\Sigma$  and a mean position  $\mu$  as,

$$G(x) = e^{-\frac{1}{2}(x-\mu)^T \Sigma^{-1}(x-\mu)}. \quad (1)$$

The  $\Sigma$  is further decomposed into a scaling matrix  $S$  and a rotation matrix  $R$ , as  $\Sigma = RSS^T R^T$ . And  $S$  and  $R$  are optimized with two learnable vectors  $s \in \mathbb{R}^3$  for scaling and  $r \in \mathbb{R}^4$  for rotation. For modeling of the appearance, each Gaussian also contains the spherical harmonics (SH) and opacity  $\alpha$  information. In summary, a 3D Gaussian consists of the following parameters as  $G = \{\mu, r, s, SH, \alpha\}$ .

With a set of 3D Gaussians and a given view direction  $P$ , the corresponding 2D image  $I$  is rendered with the differentiable splatting-based rasterizer  $\mathcal{R}$  as,

$$I = \mathcal{R}(G, P). \quad (2)$$

By calculating the  $\mathcal{L}_{L1} = L1(I, \hat{I})$  loss between the rendered image  $I$  and the ground truth  $\hat{I}$ , the traditional 3DGS backpropagates the gradient, and iteratively updates the Gaussian parameters, until they adapt to the geometry of the target scene.

**Dynamic Gaussian Splatting for Talking Head.** 3DGS is designed for modeling static scenes, resulting in a fixed state for the 3D Gaussian points after optimization. For the talking head synthesis task in this work, the positions, colors, and other attributes of the 3D Gaussian points needed to be continuously adjusted based on the input audio signals, particularly in the highly dynamic mouth region. Therefore, we incorporate audio signals into the modeling of Gaussian Splatting for dynamic and temporally coherent talking head

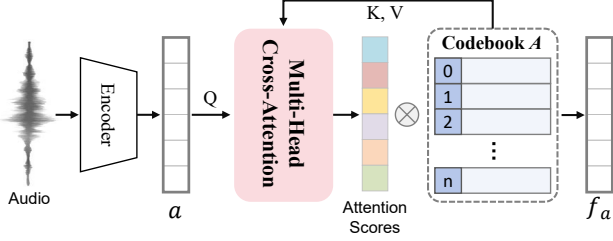


Figure 3. Illustration of the cross-attention module.

animation. To effectively incorporate the temporal information, we utilize a two-stage smoothing operation in the audio encoder. The raw audio signal is first segmented into overlapping windows of 16 time intervals as VOCA [10]. Then the pre-trained RNN-based DeepSpeech [16] is employed to extract per-frame audio features. Adjacent features are further fused into  $a$  with a temporal filtering [34] for inter-frame consistency. With audio feature  $a$  and Gaussian position  $(x, y, z)$  as the input, this 4D scene  $G'$  can be simply formulated with a deformation module  $\mathcal{F}$  as,

$$G' = G + \Delta G = G + \mathcal{F}(G, a, x, y, z), \quad (3)$$

where  $\Delta G = \mathcal{F}(G, a, x, y, z)$  is the deformations of Gaussians. The next subsection will detail the designed deformation module  $\mathcal{F}$ .

### 3.3. Audio Factorization Plane

With the overall learning process in Eq. 3, the primary task now lies in designing the module  $\mathcal{F}$  to optimally integrate audio  $a$  and spatial information  $(x, y, z)$ . One possible solution is to extract audio features and spatial features separately, and then combine them for learning, as Figure 1 (a). This approach explicitly models the 3D spatial field, and relies on an MLP to implicitly learn the audio-conditioned dynamic field, which increases the difficulty of learning. This motivates us to propose an explicit representation for the audio-driven 4D volume.

Storing a 4D volume directly is memory-consuming due to the curse of dimensionality. To avoid this, we propose the Audio Factorization Plane (Audio-Plane), a new compact and interpretable feature representation for the audio-driven dynamic field. Specifically, to reduce the computational dimension, we factorize the 4D volume representation into three audio-independent space planes  $P_{XY}, P_{XZ}, P_{YZ}$  and three audio-dependent planes  $P_{ZA}, P_{YA}, P_{XA}$  as shown in Figure 2. The spatially correlated feature planes  $P_{XY}, P_{XZ}, P_{YZ} \in \mathbb{R}^{H \times H \times D}$  follow the traditional spatial representation [4], where  $H$  is the grid resolution and  $D$  is the feature dimension. Following we focus on introducing the audio-spatially correlated planes  $P_{ZA}, P_{YA}, P_{XA}$ , which are also the core innovation of our method.

The key challenge in constructing the audio-dependent planes is that audio features are not scalar values, making

them difficult to represent directly as a dimension. To address this, we further factorize audio-dependent planes into an audio feature grid along with three spatial feature grids. The audio grid is in the form of a learnable audio prototype grid  $A \in \mathbb{R}^{H \times D}$ , which can be seen as an audio codebook as shown in Figure 2. In parallel, we construct three spatial grid embeddings  $L_X, L_Y, L_Z \in \mathbb{R}^{H \times D}$  corresponding to each spatial dimension. These paired feature grids are then employed to span three audio-spatially correlated feature planes. Participially, for a 3D Gaussian point  $(x, y, z)$  with conditioned audio  $a$ , we design a cross-attention module to obtain its audio representation  $f_a \in \mathbb{R}^D$  from the audio feature grid  $A$ , as shown in Figure 3. In this attention module, the input audio  $a$  acts as the *query* information, while the audio grid  $A$  is employed as the *key* and *value*. The specific cross-attention process is formulated as,

$$f_a = \text{Attention}(Q, K, V) = \text{Softmax} \left( \frac{QK^T}{\sqrt{d_k}} \right) V, \quad (4)$$

where  $\sqrt{d_k}$  is the scaling factor.  $Q, K, V$  are queries, keys, and values, with  $K = V = A$  and  $Q = a$ . Subsequently, we can also obtain the spatial embedding of this Gaussian point on  $L_Z$  feature grid through bilinear interpolation, as  $f_z \in \mathbb{R}^D$ . On this basis, the representation of this Gaussian point on  $P_{ZA}$  feature plane is formulated as,

$$f_{za} = f_z \cdot f_a. \quad (5)$$

For features on the other two planes  $P_{YA}$  and  $P_{XA}$ , the operation is the same. In this way, the audio feature grid  $A$  pairing with each spatial feature grid  $L_X, L_Y, L_Z$  can span the audio-spatial correlation feature planes. It's worth noting that such audio factorization 'plane' is spanned with two feature grids rather than a real feature plane, and we depict these planes with dashed lines in Figure 2 for annotation. This design provides sufficient capacity to capture intricate temporal-spatial dependencies with compact representation, enhancing the model's ability to represent dynamic audio-driven lip movements.

In practice, we use multi-resolution feature planes. In summary, the Audio-Plane comprises  $\{P_{XY}^s, P_{XZ}^s, P_{YZ}^s, L_X^s, L_Y^s, L_Z^s, A^s\}$ , where  $s$  is the upsampling scale,  $P_{XY}^s \in \mathbb{R}^{sH \times sH \times D}$ ,  $L_X^s \in \mathbb{R}^{sH \times D}$ ,  $A^s \in \mathbb{R}^{sH \times D}$  and so on. On this basis, the process for computing feature  $f$  of a Gaussian point from the proposed Audio-Plane can be formulated as,

$$f = \bigcup_{(s)} \bigcup_{(i,j,k)} (\text{Interp}(P_{ij}^s) \cdot (f_k^s) \cdot f_a^s), \quad (6)$$

where  $(i, j, k) \in \{(X, Y, Z), (X, Z, Y), (Y, Z, X)\}$ ,  $s \in \{1, 2, 3, 4\}$ . 'Interp' indicates the bilinear interpolation. The symbol ' $\bigcup$ ' denotes the concatenate operation.

Based on the learned audio-aware spatial feature  $f$ , an MLP network  $\mathcal{D}_1$  is employed to obtain the Gaussian deformation as  $\Delta G = \mathcal{D}_1(f)$ . In this way, we enable the control

of 3D Gaussians with audio signals, extending it to dynamic talking head modeling.

### 3.4. Dynamic Splatting

With the Audio-Plane introduced above, we couple audio with spatial information to guide the dynamic learning of Gaussian points. However, such a deformation learning strategy treats all facial regions uniformly, despite the fact that different regions of the face exhibit significantly varying levels of dynamic frequency. This motivates us to design a region-aware deformation field to address the varying dynamic characteristics across different facial regions. For the highly dynamic mouth region, we aim for the model to capture rich deformations, while for other relatively static facial areas, we de-emphasize dynamic learning.

To this end, we propose to assign a dynamic parameter  $d$  to each Gaussian point, which controls the degree of dynamic variation. The  $d \in \mathbb{R}^1$  is learned from the audio-aware spatial feature  $f$  with a tiny MLP network  $\mathcal{D}_2$  as  $d = \mathcal{D}_2(f)$ . Denote the dynamic weights of all Gaussians as  $D = \{d\}$ , then the final Gaussian  $G'$  is represented as,

$$G' = G + D \cdot \Delta G. \quad (7)$$

Then the challenge is how to apply region-aware supervision for the learning of  $d$ . Due to the unordered nature of the spatial Gaussian points, it is complicated to determine which specific facial region each Gaussian point corresponds to. We therefore propose the dynamic splatting method as shown in Figure 2. Specifically, the dynamism weights of all Gaussians  $D$  are mapped back into the 2D image space with view direction  $P$  through the differentiable splatting-based rasterizer  $\mathcal{R}$ , creating a grayscale dynamic map  $g$  which has the same size as face images,

$$g = \mathcal{R}(D, P). \quad (8)$$

The gray value in  $g$  corresponds to the dynamic weights of Gaussians in the corresponding 3D space. We further design reference masks  $m$  as shown in Figure 2, which shape are obtained by performing a dilation operation based on the mouth mask. These masks  $m$  provide region guidance for the distribution of dynamic weight. By constraining the similarity between the grayscale map  $g$  and the reference mask  $m$  of the corresponding frame, we lead the model to assign higher dynamic weights to Gaussian points in the mouth region with frequent dynamics. Furthermore, since the mask image represents an absolute 0-1 distribution, whereas the actual dynamism weights are not strictly binary, we design this loss  $\mathcal{L}_{\text{mask}}$  with a margin as,

$$\mathcal{L}_{\text{mask}} = \max(0, \|m - g\| - \text{margin}). \quad (9)$$

This strategy allows the dynamism weight  $d$  to adjust adaptively within a certain range, ensuring that  $d$  can vary smoothly instead of being restricted to a binary state.

The proposed dynamic splatting method helps our model to more intensively model the dynamics of the mouth while minimizing unnecessary complexity in less dynamic face regions, which can enhance the accuracy of audio-lip synchronization.

### 3.5. Training Objectives

We follow the practice in 3DGS to divide the training process into the coarse and fine training stages. In the coarse training phase, the facial dynamics are not modeled. The training objective is the L1 loss and the LPIPS loss to compare the generated images with the real ones, as  $\mathcal{L}_{\text{coarse}} = \mathcal{L}_{L1} + \lambda_{\text{LPIPS}} \mathcal{L}_{\text{LPIPS}}$ . This provides a good initialization for the Gaussian points, enabling them to roughly fit the basic shape of the face. In the fine training phase, we introduce the AP-Plane and the dynamic splatting to model the dynamics of talking faces under audio control. An additional loss  $\mathcal{L}_{\text{mask}}$  is contained to supervise the region-aware deformation field. Therefore the loss objective in the fine training stage is  $\mathcal{L}_{\text{fine}} = \mathcal{L}_{L1} + \lambda_{\text{LPIPS}} \mathcal{L}_{\text{LPIPS}} + \lambda_{\text{mask}} \mathcal{L}_{\text{mask}}$ .

## 4. Experiments

### 4.1. Experimental Settings

**Dataset.** We use the video clips publicly released in some previous methods [15, 28] as the datasets for experiments. These high-resolution videos are captured in real life scene with an average length of 4 minutes, allowing us to evaluate the performance of talking head generation methods in practical application scenarios. We set the video Frame Per Second (FPS) to 25, the resolution to  $512 \times 512$ , and extracted the head pose through the face tracking tool in [33].

**Metric.** We assess the performance of our proposed method using a combination of visual results and quantitative indicators. The primary metrics for evaluating image quality include PSNR ( $\uparrow$ ), SSIM ( $\uparrow$ ) [37] and LPIPS ( $\downarrow$ ) [45]. PSNR and SSIM are traditional measures that assess the fidelity and structural similarity of the generated images compared to the ground truth. LPIPS, a learning-based perceptual similarity measure, aligns more closely with human perception and is therefore recommended as a more objective indicator. To evaluate the audio-visual synchronization quality, which is crucial for the audio-driven talking head generation task, we use the SyncNet Confidence score ( $\uparrow$ ) [9]. In our notation, a higher score ' $\uparrow$ ' indicates better performance for PSNR, SSIM, and SyncNet Confidence, while a lower score ' $\downarrow$ ' is preferred for LPIPS.

**Implementation Details.** In the coarse training phase, we randomly initialize 1,000 Gaussian points and train for 3,000 iterations to optimize the Gaussian points. In the fine training stage, we jointly optimize both the Gaussian points, the Audio-Plane, and the deformation field for 100,000 iterations. The feature dimensions are  $D = 16$ , the size of

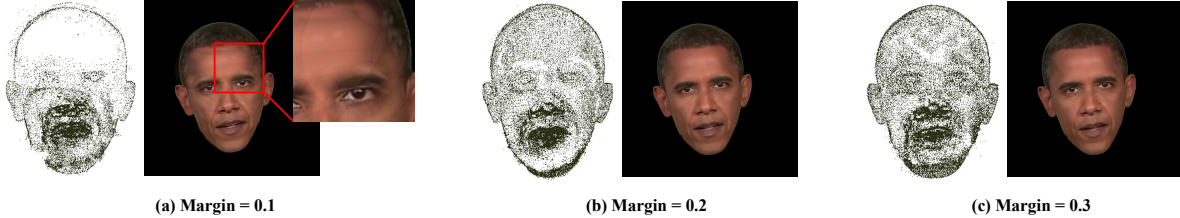


Figure 4. Generated results and the corresponding point clouds under different margins.

Method	PSNR $\uparrow$	SSIM $\uparrow$	LPIPS $\downarrow$	SyncNet $\uparrow$
GT	-	-	-	9.175
w/o A&D	30.73	0.920	0.041	4.565
w/o A	30.81	0.923	0.039	5.427
w/o D	31.54	0.925	0.037	6.342
All (Ours)	<b>31.69</b>	<b>0.929</b>	<b>0.035</b>	<b>6.700</b>

Table 1. Ablation study on the contribution of the proposed Audio-Plane (‘A’) and the Dynamic Splatting (‘D’).

Backbone	Fusion	PSNR $\uparrow$	LPIPS $\downarrow$	SyncNet $\uparrow$
GT	-	-	-	8.266
MLP	multiply	31.43	0.093	4.447
	add	32.10	0.043	4.915
	concat	32.22	0.043	5.149
Cross-Attention	multiply	31.65	0.052	5.170
	add	32.37	0.042	5.230
	concat	<b>32.88</b>	<b>0.038</b>	<b>5.518</b>

Table 2. Impact of different designs of the Audio-Plane.

the feature plane is  $H = 64$ . We set the loss weight as  $\lambda_{\text{LPIPS}} = 0.05$  and  $\lambda_{\text{mask}} = 0.1$ , and the margin in  $\mathcal{L}_{\text{mask}}$  is set as 0.2, which are selected according to the experiments. During inference, the synthesized head part is combined with the torso part and background to produce the final result. All experiments are conducted on one NVIDIA 3090Ti GPU.

## 4.2. Ablation Study

**Effect of the Audio-Plane and Dynamic Splatting.** In this section, we investigate the effect of the proposed Audio Factorization Plane (denoted as ‘A’) and the dynamic splatting (denoted as ‘D’) as Table 1. In the ‘w/o A&D’ setting, the audio feature is directly concatenated with spatial embedding to drive a Gaussian Splatting model. Results in Table 1 show that introducing the dynamic splatting method boosts the LPIPS to 0.039 and SyncNet to 5.427, indicating better perceptual quality and audio-lip synchronization. This improvement is attributed to the deformation field’s ability in

Margin	PSNR $\uparrow$	SSIM $\uparrow$	LPIPS $\downarrow$	SyncNet $\uparrow$
GT	-	-	-	6.915
0.05	31.76	0.943	0.062	4.443
0.1	32.02	0.950	0.047	4.760
0.2	31.95	<b>0.954</b>	<b>0.042</b>	<b>5.176</b>
0.3	<b>32.20</b>	0.952	<b>0.042</b>	4.615

Table 3. Impact of different selections of margin in  $\mathcal{L}_{\text{mask}}$ .

finer region-aware deformation modeling. The Audio-Plane enhances LPIPS to 0.037 and SyncNet to 6.342, since it provides a more compact feature representation for the audio-driven head, resulting in more coherent and synchronized lip movements with the audio track. The combination of the dynamic splatting and Audio-Plane yields superior results, demonstrating the effect of our proposed method.

**Different Designs in Audio-Plane.** In the proposed Audio-Plane, we design a cross-attention module to get the attention scores as Figure 3. In this section, we compare the performance when replacing the attention module with an MLP network to directly predict the attention scores. The Audio-Plane comprises three sets of feature planes (e.g.  $P_{XY}$  and  $P_{ZA}$  is a set of grids), and the fusion mode of these three sets of features has a certain influence on the experimental results. Here we explore three fusion strategies including *Multiply*, *Add*, and *Concatenate*. The results of two backbones with three fusion modes are shown in Table 2, where the cross-attention backbone combined with concatenation fusion mode is consistently superior to other methods.

**Investigation on Margin Selections for the Dynamic Splatting.** In the design of the dynamic splatting, we use mouth mask images for supervision. However, the actual dynamic weights do not absolutely follow the 0-1 binary distribution. We therefore present the margin-based  $\mathcal{L}_{\text{mask}}$  as Eq. 9. Here we investigate the impact of different margins in  $\mathcal{L}_{\text{mask}}$ . Quantitative results in Table 3 illustrate that setting the margin as 0.2 can obtain the comprehensive optimal result. In Figure 4, we further visualize the generated face image and the corresponding point clouds under different margins. It can be seen that with the dynamic splatting strategy, there are more dense Gaussian points in the dy-

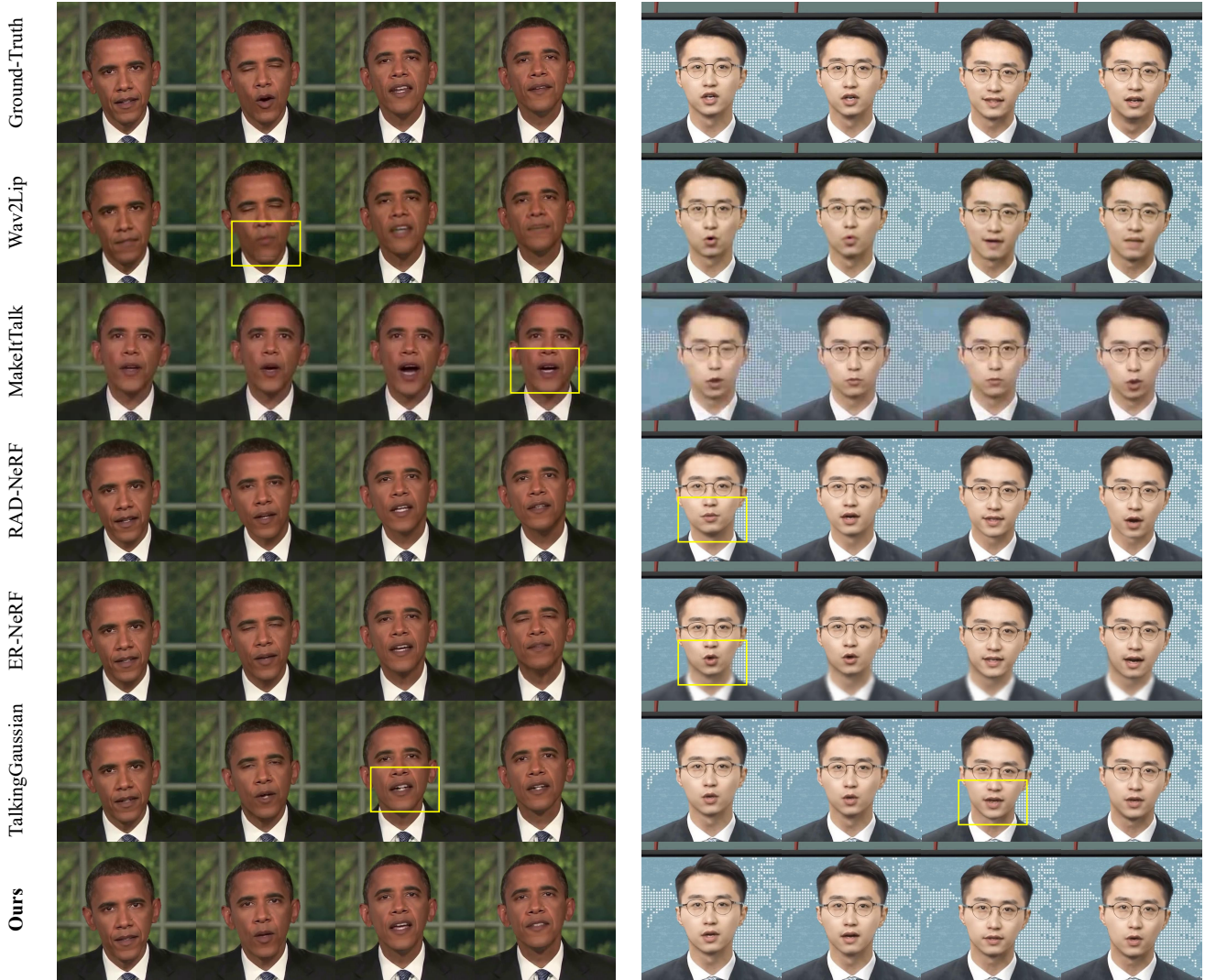


Figure 5. Visual comparison with some representative talking head synthesis methods, including 2D-based ones Wav2lip [27] and MakeItTalk [47], NeRF-based ones RAD-NeRF [32] and ER-NeRF [19], and Gaussian Splatting-based TalkingGaussian [20].

namically active mouth region. A lower margin as Figure 4 (a) results in sparser point clouds, leading to artifacts in the synthesized face, as highlighted in the zoomed-in view for clarity. However, when the margin is set too high at 0.3, the aggregation of Gaussian points in the mouth region decreases, and these points are more evenly distributed across the face as shown in (c), which is not conducive to the focus modeling of the mouth movement. We therefore choose an appropriate margin of 0.2 in the experiments.

### 4.3. Method Comparison

In this section, we compare our proposed method with some popular talking head synthesis approaches, including 2D-based MakeItTalk [47] and Wav2Lip [27], NeRF-based AD-NeRF [15], RAD-NeRF [32] and ER-NeRF [19], and Gaussian Splatting-based methods GaussianTalker [7] and

TalkingGaussian [20]. The evaluation is conducted on two test sets, with metrics for visual quality, audio-visual synchronization and rendering speed FPS (Frames Per Second). Figure 5 shows the visual comparison with some representative methods. We used yellow boxes to highlight some inaccurate mouth shapes or artifacts. We observe that the facial animations generated by our Audio-Plane closely match the ground-truth videos, demonstrating its superior ability to model dynamic facial movements. In comparison, MakeItTalk [47] and Wav2Lip [27] perform relatively poorly in visual quality with some mismatch in the mouth shape. RAD-NeRF [32] and ER-NeRF [19] produce relatively high image quality, whereas inaccurate lip shapes still appear. TalkingGaussian [20] model the inside mouth and the head part separately, leading to some teeth area artifacts.

We further conduct a comprehensive quantitative com-

Method	Test Set A				Test Set B				FPS
	PSNR $\uparrow$	SSIM $\uparrow$	LPIPS $\downarrow$	SyncNet $\uparrow$	PSNR $\uparrow$	SSIM $\uparrow$	LPIPS $\downarrow$	SyncNet $\uparrow$	
GT	-	-	-	9.175	-	-	-	8.266	-
MakeItTalk [47]	29.46	0.908	0.092	5.647	31.75	0.945	0.042	4.906	10
Wav2Lip [27]	31.58	0.913	0.082	<b>8.554</b>	32.58	0.951	0.092	<b>8.044</b>	15
AD-NeRF [15]	<u>31.65</u>	0.922	0.082	4.311	32.33	<u>0.953</u>	0.048	4.321	0.1
RAD-Nerf [32]	30.20	<u>0.927</u>	0.041	6.537	<u>32.86</u>	0.946	<u>0.039</u>	5.323	32
ER-Nerf [19]	29.66	0.921	<u>0.037</u>	6.549	32.83	0.944	0.041	5.124	34
GaussianTalker [7]	29.05	0.913	0.042	6.438	30.16	0.922	0.043	5.059	20
TalkingGaussian [20]	28.92	0.910	0.043	5.026	30.83	0.923	0.042	5.405	<b>45</b>
<b>Ours</b>	<b>31.69</b>	<b>0.929</b>	<b>0.035</b>	<u>6.700</u>	<b>32.88</b>	<b>0.956</b>	<b>0.038</b>	<u>5.518</u>	<b>43</b>

Table 4. Comparison with some representative talking head synthesis methods on two test sets. We show the best and second best results with **bold** and underline, respectively. Our method achieves real-time rendering speed with comprehensive optimal results on visual quality and audio-visual synchronization metrics.

Driven Audio	Same Id.	English (M)	Chinese (M)	French (F)	German (F)
English (M)	5.518	4.900	4.499	4.344	4.980
Chinese (M)	5.895	4.605	5.216	3.741	4.812
French (M)	5.143	3.460	4.033	5.017	4.069

Table 5. SyncNet scores under the cross language setting

parison as shown in Table 4. We show the best and second best results with **bold** and underline, respectively. It can be seen that our method achieves the best LPIPS score of 0.035 on Test Set A, and 0.038 on Test Set B. Our SyncNet scores are the 2<sup>nd</sup> best, only inferior to Wav2Lip. Although Wav2lip gets the best SyncNet score, it underperforms in terms of faithful reconstruction, reflected in its lower LPIPS scores. This can also be clearly observed in the supplementary video. Moreover, our method can render frames at a speed of 43 fps. With videos typically running at 25 fps, our method’s rendering capability of 43 fps demonstrates its strong potential for real-time applications.

Overall, our Audio-Plane consistently achieves the best or second-best scores across all metrics, demonstrating its comprehensive superiority in generating high-quality, synchronized, and real-time talking head videos. Additionally, with videos typically running at 25 fps, our method’s rendering capability of 43 fps demonstrates its strong potential for real-time applications.

#### 4.4. Cross Language Driven Results

Benefiting from the audio feature grid design, our approach can be gracefully extended to new driven audio. To validate this, we conducted experiments in the cross language driven setting. Experimental results on SyncNet scores in Table 5 demonstrate the superiority of our method in the cross driven setting. Here we train the models of three sub-

jects and then use audio clips of four different languages to drive them. It can be seen that our approach achieves satisfactory results across different source-target language pairs, indicating robust audio-visual synchronization. Additionally, our method shows strong performance even when there are significant linguistic differences between the source and target languages. These results highlight the robustness and generalization capability of our method, making it well-suited for multilingual applications.

#### 4.5. Ethical Consideration

Talking head synthesis technology may raise several ethical concerns, particularly around misuse in deepfake creation, misinformation, and privacy invasion, as this technology can generate highly realistic content. We are committed to preventing these malicious activities and promoting positive applications of the talking head synthesis technology. We will require authorization for code access, and watermark the generated videos to clearly distinguish synthetic content from the real one. Together, these measures aim to promote positive applications of talking head synthesis technology while minimizing potential harm.

### 5. Conclusion

In this paper, we have proposed a real-time talking head synthesis method based on the dynamic Gaussian Splatting. We develop the Audio Factorization Plane, which provides a compact and interpretable audio-driven dynamic scene representation. Additionally, a dynamic splatting method is designed to explicitly supervise the dynamism of 3D Gaussian points, thereby enhancing the modeling accuracy of the highly dynamic mouth region. Our method can generate high-quality vivid talking videos in real time, demonstrating superior visual performance and rendering speed.

## References

- [1] Volker Blanz and Thomas Vetter. A morphable model for the synthesis of 3d faces. In *Annual Conference on Computer Graphics and Interactive Techniques*, 1999. 1, 2
- [2] Ang Cao and Justin Johnson. Hexplane: A fast representation for dynamic scenes. In *CVPR*, 2023. 2
- [3] Eric R Chan, Marco Monteiro, Petr Kellnhofer, Jiajun Wu, and Gordon Wetzstein. pi-gan: Periodic implicit generative adversarial networks for 3d-aware image synthesis. In *CVPR*, 2021. 2
- [4] Eric R Chan, Connor Z Lin, Matthew A Chan, Koki Nagano, Boxiao Pan, Shalini De Mello, Orazio Gallo, Leonidas J Guibas, Jonathan Tremblay, Sameh Khamis, et al. Efficient geometry-aware 3d generative adversarial networks. In *CVPR*, 2022. 2, 4
- [5] Lele Chen, Ross K Maddox, Zhiyao Duan, and Chenliang Xu. Hierarchical cross-modal talking face generation with dynamic pixel-wise loss. In *CVPR*, 2019. 2
- [6] Lele Chen, Guofeng Cui, Celong Liu, Zhong Li, Ziyi Kou, Yi Xu, and Chenliang Xu. Talking-head generation with rhythmic head motion. In *ECCV*, 2020. 1
- [7] Kyusun Cho, Jounghbin Lee, Heeji Yoon, Yeobin Hong, Jaehoon Ko, Sangjun Ahn, and Seungryong Kim. Gaussian talker: Real-time high-fidelity talking head synthesis with audio-driven 3d gaussian splatting. *arXiv*, 2024. 3, 7, 8
- [8] Michail Christos Doukas, Stefanos Zafeiriou, and Viktoriia Sharmanska. Headgan: Video-and-audio-driven talking head synthesis. *arXiv*, 2020. 1, 2
- [9] Joon Son Chung and Andrew Zisserman. Out of time: automated lip sync in the wild. In *ACCV*, 2016. 5
- [10] Daniel Cudeiro, Timo Bolkart, Cassidy Laidlaw, Anurag Ranjan, and Michael J Black. Capture, learning, and synthesis of 3d speaking styles. In *CVPR*, 2019. 4
- [11] Dipanjan Das, Sandika Biswas, Sanjana Sinha, and Brojeshwar Bhowmick. Speech-driven facial animation using cascaded gans for learning of motion and texture. In *ECCV*, 2020. 1, 2
- [12] Michail Christos Doukas, Stefanos Zafeiriou, and Viktoriia Sharmanska. Headgan: One-shot neural head synthesis and editing. In *ICCV*, 2021. 2
- [13] Sara Fridovich-Keil, Giacomo Meanti, Frederik Rahbæk Warburg, Benjamin Recht, and Angjoo Kanazawa. K-planes: Explicit radiance fields in space, time, and appearance. In *CVPR*, 2023. 2
- [14] Kuangxiao Gu, Yuqian Zhou, and Thomas Huang. Flnet: Landmark driven fetching and learning network for faithful talking facial animation synthesis. In *AAAI*, 2020. 1, 2
- [15] Yudong Guo, Keyu Chen, Sen Liang, Yongjin Liu, Hujun Bao, and Juyong Zhang. AD-NeRF: Audio driven neural radiance fields for talking head synthesis. In *ECCV*, 2021. 1, 2, 5, 7, 8
- [16] Awni Hannun, Carl Case, Jared Casper, Bryan Catanzaro, Greg Diamos, Erich Elsen, Ryan Prenger, Sanjeev Sathesh, Shubho Sengupta, Adam Coates, et al. Deep speech: Scaling up end-to-end speech recognition. *arXiv*, 2014. 4
- [17] Bernhard Kerbl, Georgios Kopanas, Thomas Leimkühler, and George Drettakis. 3d gaussian splatting for real-time radiance field rendering. *TOG*, 2023. 1, 2, 3
- [18] Jeong-gi Kwak, Yuanming Li, Dongsik Yoon, Donghyeon Kim, David Han, and Hanseok Ko. Injecting 3d perception of controllable nerf-gan into stylegan for editable portrait image synthesis. In *ECCV*, 2022. 1
- [19] Jiahe Li, Jiawei Zhang, Xiao Bai, Jun Zhou, and Lin Gu. Efficient region-aware neural radiance fields for high-fidelity talking portrait synthesis. In *ICCV*, 2023. 1, 2, 7, 8
- [20] Jiahe Li, Jiawei Zhang, Xiao Bai, Jin Zheng, Xin Ning, Jun Zhou, and Lin Gu. Talkinggaussian: Structure-persistent 3d talking head synthesis via gaussian splatting. *arXiv*, 2024. 3, 7, 8
- [21] Weichuang Li, Longhao Zhang, Dong Wang, Bin Zhao, Zhigang Wang, Mulin Chen, Bang Zhang, Zhongjian Wang, Liefeng Bo, and Xuelong Li. One-shot high-fidelity talking-head synthesis with deformable neural radiance field. In *CVPR*, 2023. 1
- [22] Zhe Li, Zerong Zheng, Lizhen Wang, and Yebin Liu. Animatable gaussians: Learning pose-dependent gaussian maps for high-fidelity human avatar modeling. *arXiv*, 2023. 2
- [23] Yuanxun Lu, Jinxiang Chai, and Xun Cao. Live speech portraits: real-time photorealistic talking-head animation. *TOG*, 2021. 1
- [24] Jonathon Luiten, Georgios Kopanas, Bastian Leibe, and Deva Ramanan. Dynamic 3d gaussians: Tracking by persistent dynamic view synthesis. *arXiv*, 2023. 2
- [25] Ben Mildenhall, Pratul P Srinivasan, Matthew Tancik, Jonathan T Barron, Ravi Ramamoorthi, and Ren Ng. Nerf: Representing scenes as neural radiance fields for view synthesis. In *ECCV*, 2020. 1, 2
- [26] Michael Niemeyer, Lars Mescheder, Michael Oechsle, and Andreas Geiger. Differentiable volumetric rendering: Learning implicit 3d representations without 3d supervision. In *CVPR*, 2020. 2
- [27] KR Prajwal, Rudrabha Mukhopadhyay, Vinay P Namboodiri, and CV Jawahar. A lip sync expert is all you need for speech to lip generation in the wild. In *ACM MM*, 2020. 1, 2, 7, 8
- [28] Shuai Shen, Wanhua Li, Zheng Zhu, Yueqi Duan, Jie Zhou, and Jiwen Lu. Learning dynamic facial radiance fields for few-shot talking head synthesis. In *ECCV*, 2022. 2, 5
- [29] Shuai Shen, Wanhua Li, Xiaoke Huang, Zheng Zhu, Jie Zhou, and Jiwen Lu. Sd-nerf: Towards lifelike talking head animation via spatially-adaptive dual-driven nerfs. *TMM*, 2023. 2
- [30] Linsen Song, Wayne Wu, Chen Qian, Ran He, and Chen Change Loy. Everybody’s talkin’: Let me talk as you want. *arXiv*, 2020. 2
- [31] Supasorn Suwajanakorn, Steven M Seitz, and Ira Kemelmacher-Shlizerman. Synthesizing obama: learning lip sync from audio. *TOG*, 2017. 2
- [32] Jiaxiang Tang, Kaisiyuan Wang, Hang Zhou, Xiaokang Chen, Dongliang He, Tianshu Hu, Jingtuo Liu, Gang Zeng, and Jingdong Wang. Real-time neural radiance talking portrait synthesis via audio-spatial decomposition. *arXiv*, 2022. 1, 2, 7, 8

- [33] Justus Thies, Michael Zollhofer, Marc Stamminger, Christian Theobalt, and Matthias Nießner. Face2face: Real-time face capture and reenactment of rgb videos. In *CVPR*, 2016. 1, 5
- [34] Justus Thies, Mohamed Elgharib, Ayush Tewari, Christian Theobalt, and Matthias Nießner. Neural voice puppetry: Audio-driven facial reenactment. In *ECCV*, 2020. 2, 4
- [35] Konstantinos Vougioukas, Stavros Petridis, and Maja Pantic. Realistic speech-driven facial animation with gans. *IJCV*, 2020. 2
- [36] Ting-Chun Wang, Arun Mallya, and Ming-Yu Liu. One-shot free-view neural talking-head synthesis for video conferencing. In *CVPR*, 2021. 1
- [37] Zhou Wang, Alan C Bovik, Hamid R Sheikh, and Eero P Simoncelli. Image quality assessment: from error visibility to structural similarity. *TIP*, 2004. 5
- [38] Guanjun Wu, Taoran Yi, Jiemin Fang, Lingxi Xie, Xiaopeng Zhang, Wei Wei, Wenyu Liu, Qi Tian, and Xinggang Wang. 4d gaussian splatting for real-time dynamic scene rendering. *arXiv*, 2023. 1, 2
- [39] Wayne Wu, Yunxuan Zhang, Cheng Li, Chen Qian, and Chen Change Loy. Reenactgan: Learning to reenact faces via boundary transfer. In *ECCV*, 2018. 2
- [40] Hongyi Xu, Guoxian Song, Zihang Jiang, Jianfeng Zhang, Yichun Shi, Jing Liu, Wanchun Ma, Jiashi Feng, and Linjie Luo. Omniaavatar: Geometry-guided controllable 3d head synthesis. In *CVPR*, 2023. 2
- [41] Zeyu Yang, Hongye Yang, Zijie Pan, Xiatian Zhu, and Li Zhang. Real-time photorealistic dynamic scene representation and rendering with 4d gaussian splatting. In *ICLR*, 2024. 2
- [42] Shunyu Yao, RuiZhe Zhong, Yichao Yan, Guangtao Zhai, and Xiaokang Yang. Dfa-nerf: Personalized talking head generation via disentangled face attributes neural rendering. *arXiv*, 2022. 1, 2
- [43] Hongyun Yu, Zhan Qu, Qihang Yu, Jianchuan Chen, Zhonghua Jiang, Zhiwen Chen, Shengyu Zhang, Jimin Xu, Fei Wu, Chengfei Lv, et al. Gaussiantalker: Speaker-specific talking head synthesis via 3d gaussian splatting. In *ACMMM*, 2024. 3
- [44] Egor Zakharov, Aliaksandra Shysheya, Egor Burkov, and Victor Lempitsky. Few-shot adversarial learning of realistic neural talking head models. In *ICCV*, 2019. 1
- [45] Richard Zhang, Phillip Isola, Alexei A Efros, Eli Shechtman, and Oliver Wang. The unreasonable effectiveness of deep features as a perceptual metric. In *CVPR*, 2018. 5
- [46] Xi Zhang, Xiaolin Wu, Xinliang Zhai, Xianye Ben, and Chengjie Tu. Davd-net: Deep audio-aided video decompression of talking heads. In *CVPR*, 2020. 1
- [47] Yang Zhou, Xintong Han, Eli Shechtman, Jose Echevarria, Evangelos Kalogerakis, and Dingzeyu Li. Makelttalk: speaker-aware talking-head animation. *TOG*, 2020. 1, 2, 7, 8
- [48] Michael Zollhöfer, Justus Thies, Pablo Garrido, Derek Bradley, Thabo Beeler, Patrick Pérez, Marc Stamminger, Matthias Nießner, and Christian Theobalt. State of the art on monocular 3d face reconstruction, tracking, and applications. In *Computer Graphics Forum*, 2018. 1
- [49] Matthias Zwicker, Hanspeter Pfister, Jeroen Van Baar, and Markus Gross. Surface splatting. In *SIGGRAPH*, 2001. 2